

# Observation of leaky slab modes in an air-bridged semiconductor waveguide with a two-dimensional photonic lattice

M. Kanskar, P. Paddon, V. Pacradouni, R. Morin, A. Busch, Jeff F. Young,<sup>a)</sup>  
S. R. Johnson, Jim MacKenzie, and T. Tiedje<sup>b)</sup>  
*Department of Physics and Astronomy, University of British Columbia, Vancouver,  
British Columbia V6T 1Z1, Canada*

(Received 22 July 1996; accepted for publication 10 January 1997)

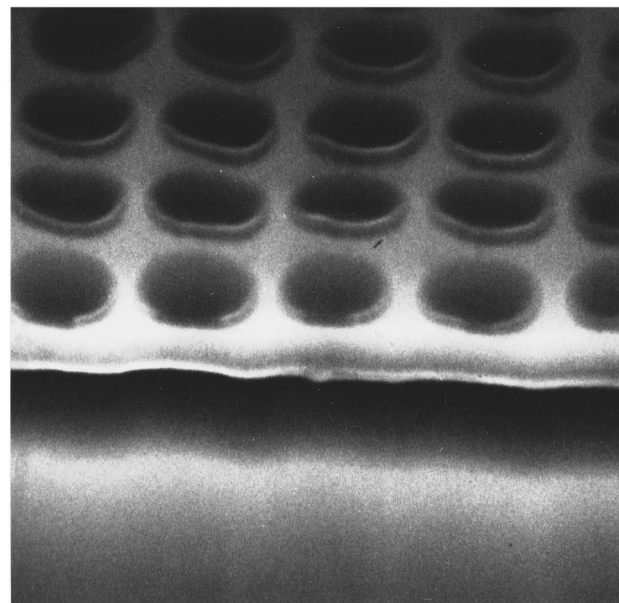
An air-bridged, 120-nm-thick semiconductor slab with a two-dimensional (2D) square array of through holes on a 480 nm pitch ( $\Lambda$ ) was fabricated using selective wet etching techniques. The second order photonic resonances of the structure were studied by comparing broadband optical scattering data with numerical solutions of Maxwell's equations. Features observed in these spectra over a  $1200\text{ cm}^{-1}$  range, near  $9500\text{ cm}^{-1}$ , indicate that the 2D texture splits the energy degeneracy of slab modes with propagation constants  $\{\pm 2\pi/\Lambda, 0\}$  and  $\{0, \pm 2\pi/\Lambda\}$  by as much as 14%. © 1997 American Institute of Physics. [S0003-6951(97)02811-8]

The distributed feedback (DFB) laser is a commercial example of how novel functionality can result from controlling the refractive index profile of a dielectric structure on length scales comparable to the operating wavelength of an optoelectronic device.<sup>1</sup> In a typical DFB laser this advantage results from a slight modification of the electromagnetic excitation spectrum of a planar waveguide structure that is induced by a small amplitude, one-dimensional (1D) periodic corrugation of the refractive index. More dramatic effects have been observed in semiconductor microcavity structures in which the physical structure itself [1D periodic in the case of small-diameter vertical cavity lasers,<sup>2</sup> and three dimensional (3D), nonperiodic in the case of microdisk lasers<sup>3</sup>] has a larger influence on the density of electromagnetic modes that interact with electronic excitations within the structure. Possible applications for this more general class of dielectric microstructures include thresholdless lasers,<sup>3</sup> single-mode-light-emitting diodes,<sup>4</sup> squeezed light generators,<sup>5</sup> and cladding layers for low-loss waveguides.<sup>6</sup>

In this letter, we present experimental results on the fabrication and optical characterization of an air-bridged semiconductor slab waveguide containing a two dimensional (2D) lattice of air holes that completely penetrate the slab. This structure, which we refer to as a porous waveguide (PW), integrates several concepts reported previously in the context of controlling the local photonic density of states over a wide spectral range.<sup>7-9</sup> We provide evidence showing that the spectral range over which the PW affects the basic optical properties of the guide is approximately two orders of magnitude larger than in a typical DFB structure.

A scanning electron micrograph of the cleave through a PW is shown in Fig. 1, and a cross-sectional schematic appears as an inset to Fig. 3(a). The structure consists of a 2D square lattice of nearly cylindrical air holes with a pitch,  $\Lambda$ , of 480 nm. The holes were obtained by wet etching the waveguide through a mask of 200-nm-thick polymethylmethacrylate (PMMA) which had been exposed by an electron beam from a 30 KeV scanning electron microscope

(SEM) over an  $80\text{ }\mu\text{m}\times 80\text{ }\mu\text{m}$  area. The air-bridge was formed by etching away the underlying  $0.85\text{-}\mu\text{m}$  thick sacrificial  $\text{Al}_{0.6}\text{Ga}_{0.4}\text{As}$  layer through the air holes using a high contrast etchant.<sup>10</sup> This process selectively removed only the  $\text{Al}_{0.6}\text{Ga}_{0.4}\text{As}$  under the patterned section of the waveguide, leaving the PW supported on its perimeter by unetched  $\text{Al}_{0.6}\text{Ga}_{0.4}\text{As}$ , and from underneath by a small number of randomly located  $\text{Al}_{0.6}\text{Ga}_{0.4}\text{As}$  mesas that resisted the etch. A cleave was then made through the air-bridged PW. The symmetric waveguide, which was grown by molecular beam epitaxy (MBE), is comprised of a single  $6.1\text{ nm}$   $\text{In}_{0.2}\text{Ga}_{0.8}\text{As}$  quantum well in the center, flanked by  $24\text{ nm}$  of GaAs and  $33\text{ nm}$  of graded  $\text{Al}_x\text{Ga}_{1-x}\text{As}$  ( $x:0.1\rightarrow 0.4$ ) on



750 nm

FIG. 1. Scanning electron micrograph of the cleaved section of a porous waveguide. This is the view looking down, from right to left, in the schematic diagram included as an inset to Fig. 3(a).

<sup>a)</sup>Electronic mail: young@physics.ubc.ca

<sup>b)</sup>Also at: Department of Electrical Engineering, University of British Columbia, Canada.

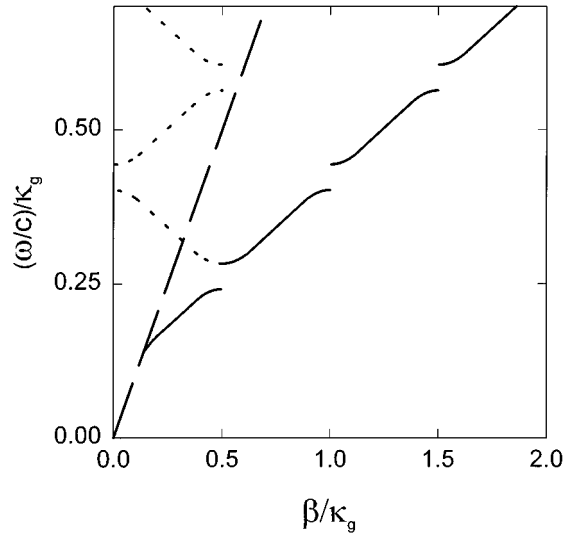


FIG. 2. The dispersion (schematic) of TE polarized guided modes in a slab waveguide containing a 1D grating with pitch  $\Lambda = 2\pi/\kappa_g$ . The solid and dotted curves show the extended zone and reduced zone representations, respectively. The dashed line is the vacuum dispersion.

each side. The GaAs and  $\text{In}_{0.2}\text{Ga}_{0.8}\text{As}$  quantum well (QW) layers were undoped.

To contrast the optical properties of this porous waveguide with those of a conventional DFB-like waveguide, first consider a DFB waveguide in terms of photonic band structure nomenclature. A weak 1D corrugation of a planar waveguide perturbs the dispersion of the slab modes of the waveguide as schematically shown for one polarization in Fig. 2. In particular there are optical “gaps” opened up when the propagation constant,  $\beta$ , is close to a multiple of  $\kappa_g/2$ , where  $\kappa_g = 2\pi/\Lambda$ . In the reduced zone scheme, eigen states below the vacuum light line remain bound modes of the textured guide while those above are “leaky modes,” or “resonant states,” because they have a finite lifetime associated with field components that couple to radiation modes.

To describe a planar waveguide with two-dimensional (2D) texture, it is necessary to deal with 2D reciprocal space where, for a square lattice, the reciprocal lattice vectors are  $\mathbf{K}_{n,m} = n2\pi/\Lambda\mathbf{x} + m2\pi/\Lambda\mathbf{y}$ . We restrict the following discussion to second order resonant states. In the 1D case, these are primarily made up of fields with wave vectors  $\boldsymbol{\beta} = \pm\kappa_g\mathbf{x}$  that are coupled to one another through the second order,  $2\kappa_g$  component of the refractive index profile. With 2D texture, the second order resonant states are primarily superpositions of four fields with wave vectors  $\boldsymbol{\beta} = \pm\kappa_g\mathbf{x}; \pm\kappa_g\mathbf{y}$ , the  $\kappa_g\mathbf{x}$  component coupling to the others through the  $2\kappa_g\mathbf{x}; \kappa_g\mathbf{x} + \kappa_g\mathbf{y}; \kappa_g\mathbf{x} - \kappa_g\mathbf{y}$  components of the refractive index profile. Thus for a square 2D lattice one expects four resonant states (per polarization) in the vicinity of the second order optical gaps. In the reduced zone scheme this corresponds to a cluster of four 2D bands, one for each resonant state, at the center of the Brillouin zone. The separation of these bands reflects the strength of the Fourier components of the refractive index modulation listed above.

We have probed the second order resonant states using radiation incident *normal* to the wafer surface. This takes advantage of the leaky nature of the second order resonant

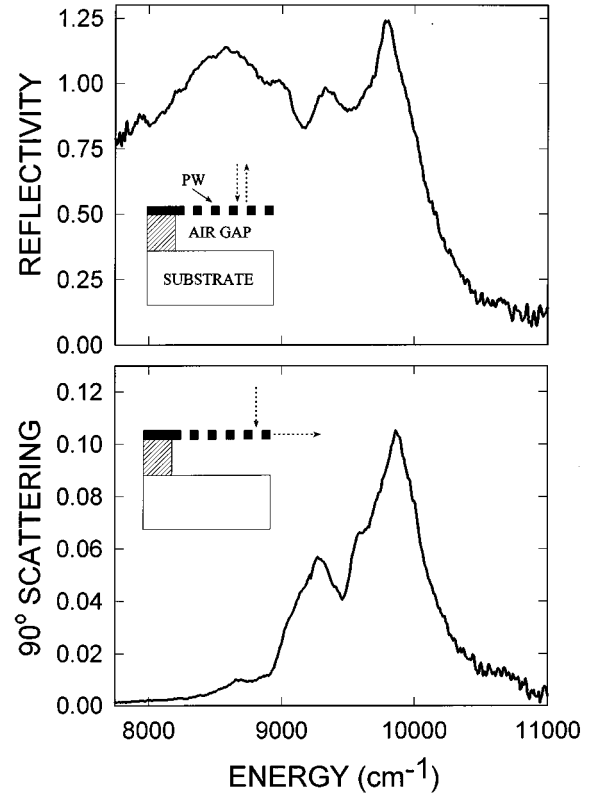


FIG. 3. (a) Normalized spectrum of normal-incidence, specular reflection from the porous waveguide surface. Inset shows the schematic of the PW, with the cleaved edge on the right, and the reflection geometry. (b) Normalized  $90^\circ$  scattered spectrum. Inset shows a schematic of the scattering geometry.

states: the *first order* Fourier components of the grating index profile couple the strong local fields of the resonant states in the PW to radiation modes with  $\beta=0$ .<sup>12</sup> A broadband (700–1600 nm) unpolarized light source was focused into one arm of a single-mode, two-into-one Y-coupled fibre and the single-ended output was imaged normally onto the top PW surface. The size of the irradiated spot was wavelength- and focus-dependent, but could be as small as  $8\ \mu\text{m}$ . The normal-incidence reflection was obtained by recording the spectrum of light reflected from the PW surface back into the second arm of the Y-coupled fiber [see arrows in inset to Fig. 3(a)]. The reflected spectrum, normalized using the reflection spectrum obtained from an untextured part of the same waveguide, is shown in Fig. 3(a). Since the reflectivity of the untextured waveguide is essentially constant over the spectral range of interest, this normalization takes into account the input spectrum and the spectral response of the collection and detection systems. The result exceeds unity in places due to absolute errors associated with the sensitivity of the reflective coupling geometry.

In a separate experiment using the same excitation conditions, the light scattered at  $90^\circ$  to the incident beam, in the basal plane of the waveguide along the [10] direction of the square lattice, was imaged into the spectrometer through a polarizer [see arrows in inset to Fig. 3(b)]. The spectrum in Fig. 3(b) is from scattered light with an electric field vector in the basal plane: very little scattered light was obtained for the orthogonal polarization. In this geometry, the strongest

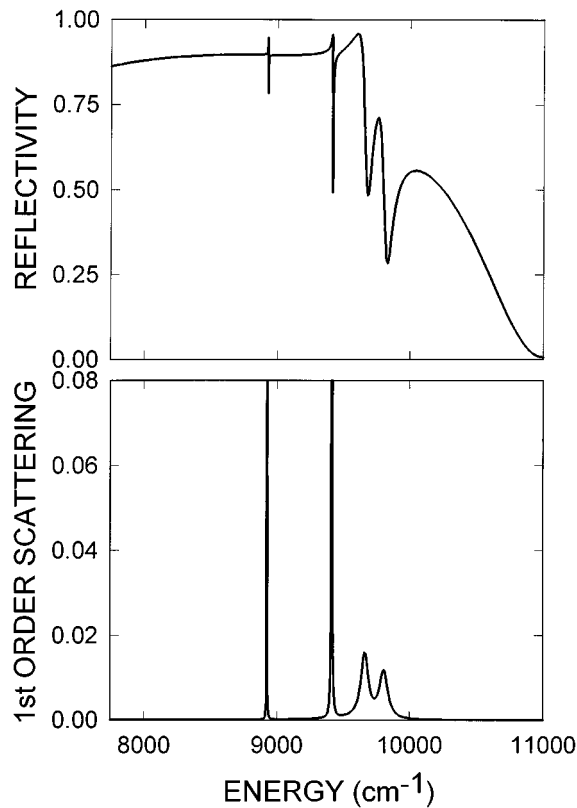


FIG. 4. (a) Calculated normal-incidence, specular reflection spectrum. (b) Calculated first order scattering amplitudes for normal-incidence radiation.

signal was achieved with the excitation spot focused close to the cleaved edge, but negligible scattered light was detected when exciting the cleaved edge of an untextured part of the sample.

The light scattered at  $90^\circ$ , from the cleaved facet of the PW, signifies the excitation of strong local fields, primarily with  $\beta = \pm \kappa_g \mathbf{x}; \pm \kappa_g \mathbf{y}$ , associated with the second order, TE-like resonant states of the PW. (TM-like states with the above propagation constant do not exist in the energy range examined experimentally.) The structure in the  $90^\circ$  and the normal-incidence reflectivity spectra are correlated with each other, and both represent the influence of the TE-like states on the scattering properties of the PW. It is clear from the experimental results that this influence extends over a broad range of frequencies, nearly  $1200 \text{ cm}^{-1}$ .

A detailed analysis of our solution of Maxwell's equations for the PW structure will be presented elsewhere.<sup>11</sup> Based on these calculations, Fig. 4(a) shows the reflectivity spectrum, and Fig. 4(b) shows the amplitude of the dominant,  $\beta = \kappa_g$ , component of the excited local fields, for plane wave radiation normally incident on a square 2D PW consisting of cylinders with a radius of 130 nm, on a pitch of 480 nm. The four TE resonant states are associated with the four peaks in the first order scattering amplitudes, easily

identified in Fig. 4(b). As in the 1D case,<sup>12</sup> resonant coupling to leaky slab modes manifests itself in the specular reflectivity as bipolar perturbations of the nominal reflectivity as shown in Fig. 4(a). A direct comparison of our theoretical model with experiment is not possible at this time mainly due to the fact that the "normally" incident radiation consisted of a tightly focused spot on the PW. The corresponding range of incident wave vectors in the experiment affects, even qualitatively, the experimental results as compared to the theory. Nevertheless, the model accurately predicts the location and range over which the texture modifies the scattering properties of the PW, and it provides useful insight as to the nature of these modifications.

In summary, both experiments and model calculations suggest that the degeneracy of guided modes with propagation constants  $[\pm \kappa_g, 0]$  and  $[0, \pm \kappa_g]$  in a 2D porous waveguide can be split by  $\sim 1000 \text{ cm}^{-1}$ , approximately two orders of magnitude larger than the second order stop gaps achieved in conventional 1D, low-contrast DFB-like grating structures. This represents a substantial modification of the density of electromagnetic modes supported by the slab. Similar structures, derived by varying the pattern of the texturing, should offer new opportunities for both passive and active optoelectronic device development.

The authors gratefully acknowledge financial support from the Natural Science and Engineering Research Council, and from Rogers Canadian Cable Labs.

<sup>1</sup>H. Kogelnik and C. V. Shank, *J. Appl. Phys.* **43**, 2327 (1972); D. R. Scifres, R. D. Burnham, and W. Streifer, *Appl. Phys. Lett.* **26**, 48 (1975); for a comprehensive reference please see *Long-Wavelength Semiconductor Lasers*, edited by G. P. Agrawal and N. K. Dutta (Van Nostrand Reinhold, New York, 1989).

<sup>2</sup>H. Soda, K. Iga, C. Kitahara, and Y. Suematsu, *Jpn. J. Appl. Phys.* **18**, 2329 (1979).

<sup>3</sup>S. L. McCall, A. F. J. Levi, R. E. Slusher, S. J. Pearton, and R. A. Logan, *Appl. Phys. Lett.* **60**, 289 (1992); A. F. J. Levi, R. E. Slusher, S. L. McCall, T. Tanbun-Ek, D. L. Coblenz, and S. J. Pearton, *Electron. Lett.* **28**, 1010 (1992).

<sup>4</sup>E. Yablonovitch, *J. Mod. Opt.* **41**, 173 (1994).

<sup>5</sup>Y. Yamamoto, S. Machida, and W. H. Richardson, *Science* **255**, 1219 (1992).

<sup>6</sup>R. D. Meade, A. Devenyi, J. D. Joannopoulos, O. L. Alerhand, D. A. Smith, and K. Kash, *J. Appl. Phys.* **75**, 4753 (1994); for a general reference see *Photonic Crystals*, J. D. Joannopoulos, R. D. Meade, and J. N. Winn (Princeton University Press, Princeton, NJ, 1995).

<sup>7</sup>P. R. Villeneuve, S. Fan, J. D. Joannopoulos, K.-Yi Lim, G. S. Petrich, L. A. Kolodziejski, and R. Reif, *Appl. Phys. Lett.* **67**, 167 (1995).

<sup>8</sup>S. T. Ho, S. L. McCall, and R. E. Slusher, *Opt. Lett.* **18**, 909 (1993).

<sup>9</sup>J. R. Wendt, G. A. Vawter, P. L. Gourley, T. M. Brennan, and B. E. Hammons, *J. Vac. Sci. Technol. B* **11**, 2637 (1993); P. L. Gourley, J. R. Wendt, G. A. Vawter, T. M. Brennan, and B. E. Hammons, *Appl. Phys. Lett.* **64**, 687 (1994).

<sup>10</sup>L. A. Coldren and J. L. Merz, *Electron. Lett.* **21**, 559 (1985).

<sup>11</sup>We used a modified version of the algorithm described in, P. M. Bell, J. B. Pendry, L. Martin-Moreno, and A. J. Ward, *Comp. Phys. Comm.* **85**, 306 (1995), with a  $10 \times 10 \times 40$  discretized mesh.

<sup>12</sup>S. L. Chuang and J. A. Kong, *J. Opt. Soc. Am.* **73**, 669 (1983).